ACADEMIC PRESS

Available online at www.sciencedirect.com

SCIENCE DIRECT®

Journal of Sound and Vibration 261 (2003) 871–893

JOURNAL OF SOUND AND VIBRATION

www.elsevier.com/locate/jsvi

Free vibration and parametric resonance of shear deformable functionally graded cylindrical panels

J. Yang[a,b], Hui-Shen Shen[a,*]

[a] *School of Civil Engineering and Mechanics, Shanghai Jiao Tong University, 1954 Hua Shan Road, Shanghai 200030, People's Republic of China*

[b] *Department of Mechanical Engineering, Wuhan Institute of Chemical Technology, Wuhan 430073, People's Republic of China*

Received 25 February 2002; accepted 11 June 2002

Abstract

This paper investigates free vibration and dynamic instability of functionally graded cylindrical panels subjected to combined static and periodic axial forces and in thermal environment. Theoretical formulations are based on Reddy's higher order shear deformation shell theory to account for rotary inertia and the parabolic distribution of the transverse shear strains through the panel thickness. Thermal effects due to steady temperature change are included in the analysis. Material properties are assumed to be temperature dependent and graded in the thickness direction according to a power-law distribution in terms of the volume fractions of the constituents. The panel under current consideration is clamped or simply supported on two straight edges and may be either free, simply supported or clamped on the curved edges. A semi-analytical approach, which takes the advantages of one-dimensional differential quadrature approximation, Galerkin technique and Bolotin's method, is employed to determine the natural frequencies and the unstable regions of the panel. Numerical results for silicon nitride/stainless-steel cylindrical panels are given in both dimensionless tabular and graphical forms. Effects of material composition, temperature rise, panel geometry parameters, and boundary conditions on free vibration and the parametric resonance are also studied.

1. Introduction

Due to the advantages of being able to withstand severe high-temperature gradient while maintaining structural integrity, functionally graded materials (FGMs) have been receiving much more attention in engineering communities, especially in high-temperature applications such as

*Corresponding author.
E-mail address: hsshen@mail.sjtu.edu.cn (H.-S. Shen).

0022-460X/02/$ - see front matter © 2002 Elsevier Science Ltd. All rights reserved.
PII: S0022-460X(02)01015-5

nuclear reactors, space planes and chemical plants [1,2]. FGMs are microscopically inhomogeneous composites usually made from a mixture of metals and ceramics. By gradually varying the volume fraction of constituent materials, their material properties exhibit a smooth and continuous change from one surface to another, thus eliminating interface problems and mitigating thermal stress concentrations. FGMs now have been regarded as one of the most promising candidates for future intelligent composites in many engineering sectors such as aerospace, fast computers, biomedical industry, environmental sensors, etc.

Despite the evident importance in practical applications, investigations on the dynamic characteristics of FGM shell structures are still limited in number. Among those available, Loy et al. [3] investigated the free vibration of simply supported FGM cylindrical shells, which was later extended by Pradhan et al. [4] to cylindrical shells under various end supporting conditions. Gong et al. [5] presented elastic response analysis of simply supported FGM cylindrical shells under low-velocity impact. By using the finite element method and Fourier transformation technique, Han et al. [6] solved the wave motion in a FGM cylinder. Ng et al. [7] studied dynamic instability of simply supported FGM cylindrical shells, a normal-mode expansion and Bolotin's method were used to determine the boundaries of the unstable regions. In all the above studies, it was assumed that material properties follow a through-thickness variation according to a power-law distribution in terms of the volume fractions of constituents. Theoretical formulations were all based on classical shell theory, i.e., neglecting the effect of transverse shear strains. Temperature dependency of the material properties was also considered, but their numerical results were only for a simple case of an FGM shell in a fixed thermal environment.

In the present analysis, free vibration and dynamic instability of FGM cylindrical panels under combined static and periodic axial forces are studied by using a proposed semi-analytical approach. Material properties of the constituents are assumed to be non-linear functions of temperature, and graded in the thickness direction according to a power-law distribution. Reddy's higher order shear deformation shell theory [8] is employed to include the effects of rotary inertia and the parabolic distribution of the transverse shear strains through the panel thickness. The panel may be clamped or simply supported on two straight edges while the remaining two loaded curved ones may be free, simply supported or clamped. A uniform temperature change is considered. Comprehensive numerical results are provided for panels made from a mixture of silicon nitride and stainless steel. A parametric study is also undertaken, giving insight into the effects of material composition, temperature rise, axial load, boundary conditions as well as panel geometry parameters on both vibration characteristics and parametric resonance.

2. Theoretical formulations

2.1. FGM material properties

An FGM cylindrical panel with its co-ordinate system (X, Y, Z) is shown in Fig. 1, where X and Y are in the axial and circumferential directions of the panel and Z is in the direction of the inward normal to the middle surface. The origin of the co-ordinate system is located at the corner of the middle plane. The panel is of radius R, thickness h, axial length a and arc length b. We assume that the panel is made from a mixture of ceramics and metals, and the material

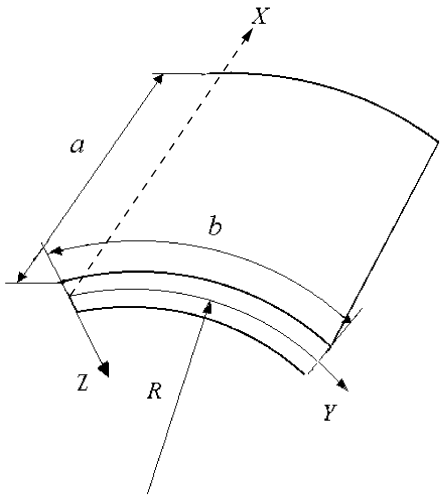

Fig. 1. Configuration of a functionally graded cylindrical panels and its co-ordinate system.

composition is continuously varied such that the top surface ($Z = -h/2$) of the panel is ceramic rich, whereas the bottom surface ($Z = h/2$) is metal rich. Thus, the effective material properties P, such as Young's modulus E, the Poisson ratio v, mass density ρ and coefficient of thermal expansion α can be expressed as

$$P = P_t V_c + P_b V_m, \tag{1}$$

in which subscript 't' and 'b' refer to the top and bottom surfaces of the panel, respectively, V_c and V_m are the ceramic and metal volume fractions, and are related by

$$V_c + V_m = 1. \tag{2}$$

The ceramic volume fraction V_c is assumed to follow a power-law distribution as

$$V_c = \left(\frac{h - 2Z}{2h}\right)^n, \tag{3}$$

where volume fraction index n characterizes the material variation profile through the panel thickness and may be varied to obtain the optimum distribution of component materials. From Eqs. (1)–(3), the effective Young's modulus E, the Poisson ratio v, mass density ρ, and thermal expansion coefficient α of an FGM panel can be expressed as

$$E = (E_t - E_b)\left(\frac{h - 2Z}{2h}\right)^n + E_b, \tag{4a}$$

$$v = (v_t - v_b)\left(\frac{h - 2Z}{2h}\right)^n + v_b, \tag{4b}$$

$$\alpha = (\alpha_t - \alpha_b)\left(\frac{h - 2Z}{2h}\right)^n + \alpha_b, \tag{4c}$$

$$\rho = (\rho_t - \rho_b)\left(\frac{h-2Z}{2h}\right)^n + \rho_b. \tag{4d}$$

Since functionally graded structures are most commonly used in high-temperature environment where significant changes in mechanical properties of the constituent materials occur [9], it is essential to take this temperature dependency into consideration for accurate prediction of the mechanical response. Therefore, E_t, E_b, v_t, v_b, ρ_t, ρ_b, α_t and α_b are functions of temperature as well, as will be shown in Section 4. This makes E, v, ρ and α both temperature and position dependent.

Thermal force resultants, thermal moment resultants and higher order thermal moment resultants due to temperature rise ΔT are defined by

$$\begin{bmatrix} \bar{N}_X^T & \bar{M}_X^T & \bar{P}_X^T \\ \bar{N}_Y^T & \bar{M}_Y^T & \bar{P}_Y^T \\ \bar{N}_{XY}^T & \bar{M}_{XY}^T & \bar{P}_{XY}^T \end{bmatrix} = \int_{-h/2}^{h/2} \begin{bmatrix} A_X \\ A_Y \\ A_{XY} \end{bmatrix} (1, Z, Z^3)\Delta T \, dZ, \tag{5}$$

where

$$\begin{bmatrix} A_X \\ A_Y \\ A_{XY} \end{bmatrix} = -\begin{bmatrix} Q_{11} & Q_{12} & Q_{16} \\ Q_{12} & Q_{22} & Q_{26} \\ Q_{16} & Q_{26} & Q_{66} \end{bmatrix} \begin{bmatrix} 1 & 0 \\ 0 & 1 \\ 0 & 0 \end{bmatrix} \begin{bmatrix} \alpha \\ \alpha \end{bmatrix}, \tag{6}$$

and

$$\begin{aligned} &Q_{11} = Q_{22} = \frac{E}{1-v^2}, \quad Q_{12} = \frac{vE}{1-v^2}, \\ &Q_{16} = Q_{26} = 0, \quad Q_{44} = Q_{55} = Q_{66} = \frac{E}{2(1+v)}. \end{aligned} \tag{7}$$

Various inertias are calculated by

$$(I_1, I_2, I_3, I_4, I_5, I_7) = \int_{-h/2}^{h/2} \left\{ (\rho_t - \rho_b)\left(\frac{h-2Z}{2h}\right)^n + \rho_b \right\} (1, Z, Z^2, Z^3, Z^4, Z^6) \, dZ. \tag{8}$$

2.2. Governing equations

We designate $\bar{U}$, $\bar{V}$ and $\bar{W}$ as the displacements in X, Y and Z directions, $\bar{\Psi}_X$ and $\bar{\Psi}_Y$ as the rotations of normals to the middle surface with respect to the Y- and X-axis, respectively. Let $\bar{F}(X, Y)$ be the stress function for the stress resultants, so that $\bar{N}_X = \bar{F}_{,YY}$, $\bar{N}_Y = \bar{F}_{,XX}$, $\bar{N}_{XY} = -\bar{F}_{,XY}$, where a comma denotes partial differentiation. Suppose the panel is initially stress free at temperature T_0, and then may be subjected to a uniform temperature rise ΔT and a periodically pulsating load in axial direction

$$p_X(t) = p_s + p_d \cos \theta t, \tag{9}$$

where p_s is a time invariant component and $p_d \cos \theta t$ is the harmonically pulsating component, θ denotes the frequency of excitation.

Based on Reddy's higher order shear deformation theory to account for the effects of rotary inertia and parabolic distribution of the transverse shear strains through thickness, the equations of motion for FGM cylindrical panels can be derived using Donnell's shell theory

$$\tilde{L}_{11}(\bar{W}) - \tilde{L}_{12}(\bar{\Psi}_X) - \tilde{L}_{13}(\bar{\Psi}_Y) + \tilde{L}_{14}(\bar{F}) - \tilde{L}_{15}(\bar{N}^{\mathrm{T}}) - \tilde{L}_{16}(\bar{M}^{\mathrm{T}}) - \frac{1}{R}\frac{\partial^2 \bar{F}}{\partial X^2} - p_X \frac{\partial^2 \bar{W}}{\partial X^2} - p_Y \frac{\partial^2 \bar{W}}{\partial Y^2} = -I_1 \ddot{\bar{W}} - \tilde{I}_5 \frac{\partial \ddot{\bar{\Psi}}_X}{\partial X} - \tilde{I}'_5 \frac{\partial \ddot{\bar{\Psi}}_Y}{\partial Y} - \tilde{I}_7 \frac{\partial^2 \ddot{\bar{W}}}{\partial X^2} - \tilde{I}'_7 \frac{\partial^2 \ddot{\bar{W}}}{\partial Y^2}, \tag{10}$$

$$\tilde{L}_{21}(\bar{F}) + \tilde{L}_{22}(\bar{\Psi}_X) + \tilde{L}_{23}(\bar{\Psi}_Y) - \tilde{L}_{24}(\bar{W}) + \frac{1}{R}\frac{\partial^2 \bar{W}}{\partial X^2} - \tilde{L}_{25}(\bar{N}^{\mathrm{T}}) = 0, \tag{11}$$

$$\tilde{L}_{31}(\bar{W}) + \tilde{L}_{32}(\bar{\Psi}_X) - \tilde{L}_{33}(\bar{\Psi}_Y) + \tilde{L}_{34}(\bar{F}) - \tilde{L}_{35}(\bar{N}^{\mathrm{T}}) - \tilde{L}_{36}(\bar{S}^{\mathrm{T}}) = -\tilde{I}_3 \ddot{\bar{\Psi}}_X + \tilde{I}_5 \frac{\partial \ddot{\bar{W}}}{\partial X}, \tag{12}$$

$$\tilde{L}_{41}(\bar{W}) - \tilde{L}_{42}(\bar{\Psi}_X) + \tilde{L}_{43}(\bar{\Psi}_Y) + \tilde{L}_{44}(\bar{F}) - \tilde{L}_{45}(\bar{N}^{\mathrm{T}}) - \tilde{L}_{46}(\bar{S}^{\mathrm{T}}) = -\tilde{I}'_3 \ddot{\bar{\Psi}}_Y + \tilde{I}'_5 \frac{\partial \ddot{\bar{W}}}{\partial Y}, \tag{13}$$

where $\bar{S}^{\mathrm{T}} = \bar{M}^{\mathrm{T}} - c_1 \bar{P}^{\mathrm{T}}$, $c_1 = 4/3h^2$, and all linear operators are defined as in Ref. [10]. A super dot implies differentiation with respect to time, and

$$\tilde{I}_3 = \bar{I}_4 - (\bar{I}_2)^2/\bar{I}_1, \quad \tilde{I}'_3 = \bar{I}'_4 - (\bar{I}'_2)^2/\bar{I}'_1,$$

$$\tilde{I}_5 = \bar{I}_5 - \bar{I}_2\bar{I}_3/\bar{I}_1, \quad \tilde{I}'_5 = \bar{I}'_5 - \bar{I}'_2\bar{I}'_3/\bar{I}'_1,$$

$$\tilde{I}_7 = (\bar{I}_3)^2/I_1 - c_1^2 I_7, \quad \tilde{I}'_7 = (\bar{I}'_3)^2/I'_1 - c_1^2 I_7,$$

$$\bar{I}_1 = I_1, \quad \bar{I}'_1 = I_1 + 2I_2/R,$$

$$\bar{I}_2 = I_2 - c_1 I_4, \quad \bar{I}'_2 = I_2 + I_3/R - c_1 I_4 - c_1 I_5/R,$$

$$\bar{I}_3 = c_1 I_4, \quad \bar{I}'_3 = c_1(I_4 + I_5/R),$$

$$\bar{I}_4 = \bar{I}'_4 = I_3 - 2c_1 I_5 + c_1^2 I_7, \quad \bar{I}_5 = \bar{I}'_5 = c_1 I_5 - c_1^2 I_7. \tag{14}$$

It is evident that $\tilde{L}_{15}(\bar{N}^{\mathrm{T}}) = \tilde{L}_{25}(\bar{N}^{\mathrm{T}}) = \tilde{L}_{35}(\bar{N}^{\mathrm{T}}) = \tilde{L}_{45}(\bar{N}^{\mathrm{T}}) = \tilde{L}_{16}(\bar{M}^{\mathrm{T}}) = \tilde{L}_{36}(\bar{S}^{\mathrm{T}}) = \tilde{L}_{46}(\bar{S}^{\mathrm{T}}) = 0$ when the temperature field varies through the panel thickness only.

Two cases of boundary conditions are considered in the analysis according to the in-plane loading conditions.

Case 1: The panel is uniformly loaded in the axial direction, clamped on the two unloaded straight edges (at $Y = 0, b$) and may have any combination of free, simply supported or clamped constraints on the loaded curved sides (at $X = 0, a$).

Case 2: In the absence of axial loading, the panel is clamped or simply supported on the two straight edges (at $Y = 0, b$) and may have any combination of free, simply supported or clamped constraints on the curved sides (at $X = 0, a$).

The associated out-of-plane boundary conditions are

$X = 0, a$:

Simply supported (S):

$$\bar{W} = 0, \quad \bar{V} = 0, \quad \bar{\Psi}_Y = 0, \quad \bar{M}_X = 0, \quad \bar{P}_X = 0. \tag{15a}$$

Clamped (C):

$$\bar{W} = 0, \quad \bar{V} = 0, \quad \bar{\Psi}_X = 0, \quad \bar{\Psi}_Y = 0, \quad \frac{\partial \bar{W}}{\partial X} = 0. \tag{15b}$$

Free (F):

$$\bar{V} = 0, \quad \bar{M}_X = 0, \quad \bar{P}_X = 0, \tag{15c}$$

$$\bar{M}^*_{XY} = \bar{M}_{XY} - c_1 \bar{P}_{XY} = 0, \quad \bar{Q}^*_X = \bar{Q}_X - 3c_1 \bar{R}_X - c_1 \left(\frac{\partial \bar{P}_X}{\partial X} + 2 \frac{\partial \bar{P}_{XY}}{\partial Y} \right) = 0. \tag{15d}$$

$Y = 0, b$:
Simply supported (S):

$$\bar{W} = 0, \quad \bar{\Psi}_X = 0, \quad \bar{M}_Y = 0, \quad \bar{P}_Y = 0, \quad \bar{N}_{XY} = 0. \tag{16a}$$

Clamped (C):

$$\bar{W} = 0, \quad \bar{\Psi}_X = 0, \quad \bar{\Psi}_Y = 0, \quad \frac{\partial \bar{W}}{\partial Y} = 0, \quad \bar{N}_{XY} = 0 \tag{16b}$$

and the in-plane boundary conditions are
$X = 0, a$:

$$\int_0^b \bar{N}_X \, \mathrm{d}Y + p_X b = 0 \ \text{(movable)} \quad \text{or} \quad \bar{U} = 0 \ \text{(immovable)}. \tag{17a}$$

$Y = 0, b$:

$$\int_0^a \bar{N}_Y \, \mathrm{d}X + p_Y a = 0 \ \text{(movable)} \quad \text{or} \quad \bar{V} = 0 \ \text{(immovable)}, \tag{17b}$$

where $\bar{M}_X$ and $\bar{M}_{XY}$ are the bending moments, $\bar{P}_X$ and $\bar{P}_{XY}$ are the higher order bending moments, $\bar{Q}_X$ and $\bar{R}_X$ stand for the transverse shear force and the higher order shear force, as defined in Ref. [8]. Note that the immovable conditions are fulfilled in an average sense as [11, 12]

$$\bar{U} = \int_0^b \int_0^a \frac{\partial \bar{U}}{\partial X} \mathrm{d}X \, \mathrm{d}Y = 0 \quad \text{at } X = 0, a, \tag{18a}$$

$$\bar{V} = \int_0^a \int_0^b \frac{\partial \bar{V}}{\partial Y} \mathrm{d}Y \, \mathrm{d}X = 0 \quad \text{at } Y = 0, b, \tag{18b}$$

and the average end shortening relationships are

$$\frac{\Delta_X}{a} = -\frac{1}{ab}\int_0^b\int_0^a \frac{\partial \bar{U}}{\partial X}\,\mathrm{d}X\,\mathrm{d}Y$$
$$= -\frac{1}{ab}\int_0^b\int_0^a \left\{\left[A_{11}^*\frac{\partial^2 \bar{F}}{\partial Y^2} + A_{12}^*\frac{\partial^2 \bar{F}}{\partial X^2} + (B_{11}^* - c_1E_{11}^*)\frac{\partial \bar{\Psi}_X}{\partial X} + (B_{12}^* - c_1E_{12}^*)\frac{\partial \bar{\Psi}_Y}{\partial Y}\right.\right.$$
$$\left.\left. -c_1\left(E_{11}^*\frac{\partial^2 \bar{W}}{\partial X^2} + E_{12}^*\frac{\partial^2 \bar{W}}{\partial Y^2}\right)\right] - \left(A_{11}^*\bar{N}_X^{\mathrm{T}} + A_{12}^*\bar{N}_Y^{\mathrm{T}}\right)\right\}\mathrm{d}X\,\mathrm{d}Y, \tag{19a}$$

$$\frac{\Delta_Y}{b} = -\frac{1}{ab}\int_0^a\int_0^b \frac{\partial \bar{V}}{\partial Y}\,\mathrm{d}Y\,\mathrm{d}X$$
$$= -\frac{1}{ab}\int_0^a\int_0^b \left\{\left[A_{22}^*\frac{\partial^2 \bar{F}}{\partial X^2} + A_{12}^*\frac{\partial^2 \bar{F}}{\partial Y^2} + (B_{21}^* - c_1E_{21}^*)\frac{\partial \bar{\Psi}_X}{\partial X} + (B_{22}^* - c_1E_{22}^*)\frac{\partial \bar{\Psi}_Y}{\partial Y}\right.\right.$$
$$\left.\left. -c_1\left(E_{21}^*\frac{\partial^2 \bar{W}}{\partial X^2} + E_{22}^*\frac{\partial^2 \bar{W}}{\partial Y^2}\right)\right] + \frac{\bar{W}}{R} - \left(A_{12}^*\bar{N}_X^{\mathrm{T}} + A_{22}^*\bar{N}_Y^{\mathrm{T}}\right)\right\}\mathrm{d}Y\,\mathrm{d}X. \tag{19b}$$

In the above equations and what follows, $[A_{ij}^*]$, $[B_{ij}^*]$, $[D_{ij}^*]$, $[E_{ij}^*]$, $[F_{ij}^*]$, $[H_{ij}^*]$ $(i,j = 1,2,6)$, are the reduced stiffness matrices and can be determined through relationships [10–12]

$$\mathbf{A}^* = \mathbf{A}^{-1},\ \ \mathbf{B}^* = -\mathbf{A}^{-1}\mathbf{B},\ \ \mathbf{D}^* = \mathbf{D} - \mathbf{B}\mathbf{A}^{-1}\mathbf{B},\ \ \mathbf{E}^* = -\mathbf{A}^{-1}\mathbf{E},$$
$$\mathbf{F}^* = \mathbf{F} - \mathbf{E}\mathbf{A}^{-1}\mathbf{B},\ \ \mathbf{H}^* = \mathbf{H} - \mathbf{E}\mathbf{A}^{-1}\mathbf{E}, \tag{20}$$

where

$$(A_{ij}, B_{ij}, D_{ij}, E_{ij}, F_{ij}, H_{ij}) = \int_{-h/2}^{h/2} Q_{ij}(1, Z, Z^2, Z^3, Z^4, Z^6)\,\mathrm{d}Z \quad (i,j = 1,2,6), \tag{21a}$$

$$(A_{ij}, D_{ij}, F_{ij}) = \int_{-h/2}^{h/2} Q_{ij}(1, Z^2, Z^4)\,\mathrm{d}Z \quad (i,j = 4,5). \tag{21b}$$

Introducing the following dimensionless quantities:

$$x = X/a,\ \ y = Y/b,\ \ \beta = a/b,\ \ t = \bar{t}\sqrt{D_{11}^*/I_1}/a^2,\ \ \omega = \Omega a^2\sqrt{I_1/D_{11}^*},$$
$$\Delta = (D_{11}^*D_{22}^*A_{11}^*A_{22}^*)^{1/4},\ \ \gamma_0 = a^2/R\Delta,\ \ W = \bar{W}/\Delta,\ \ F = \bar{F}/(D_{11}^*D_{22}^*)^{1/2},$$
$$(\Psi_x, \Psi_y) = (\bar{\Psi}_X, \bar{\Psi}_Y)a/\Delta,\ \ (\lambda_x, \lambda_y) = (p_Xb^2, p_Ya^2)/(D_{11}^*D_{22}^*)^{1/2},$$
$$(\delta_x, \delta_y) = (\Delta_X/a, \Delta_Y/b)b^2/\Delta,\ \ \gamma_{14} = [D_{22}^*/D_{11}^*]^{1/2},\ \ \gamma_{24} = [A_{11}^*/A_{22}^*]^{1/2},$$
$$\gamma_5 = -A_{12}^*/A_{22}^*,\ \ (\gamma_{T1}, \gamma_{T2}) = (A_X^{\mathrm{T}}, A_Y^{\mathrm{T}})a^2/(D_{11}^*D_{22}^*)^{1/2},$$
$$(M_x, M_y, M_{xy}, M_x^{\mathrm{T}}, M_y^{\mathrm{T}}, M_{xy}^{\mathrm{T}}) = (\bar{M}_X, \bar{M}_Y, \bar{M}_{XY}, \bar{M}_X^{\mathrm{T}}, \bar{M}_Y^{\mathrm{T}}, \bar{M}_{XY}^{\mathrm{T}})a^2/D_{11}^*\Delta,$$
$$(P_x, P_y, P_{xy}, P_x^{\mathrm{T}}, P_y^{\mathrm{T}}, P_{xy}^{\mathrm{T}}) = c_1(\bar{P}_X, \bar{P}_Y, \bar{P}_{XY}, \bar{P}_X^{\mathrm{T}}, \bar{P}_Y^{\mathrm{T}}, \bar{P}_{XY}^{\mathrm{T}})a^2/D_{11}^*\Delta,$$
$$(\hat{I}_3, \hat{I}'_3, \hat{I}_5, \hat{I}'_5, \hat{I}_7, \hat{I}'_7) = (\tilde{I}_3, \tilde{I}'_3, \tilde{I}_5, \tilde{I}'_5, \tilde{I}_7, \tilde{I}'_7)/I_1a^2 \tag{22}$$

in which Ω denotes the natural frequency of the panel, and $A_X^T(=A_Y^T)$ are defined by

$$(A_X^T, A_Y^T) = -\int_{-h/2}^{h/2} (A_X, A_Y)\,\mathrm{d}Z. \tag{23}$$

Thus, the axial pulsating load can be rewritten in dimensionless form as

$$\lambda_x = \lambda_s + \lambda_d \cos\theta t. \tag{24}$$

Also, governing Eqs. (10)–(13) can be transformed as

$$L_{11}(W) - L_{12}(\Psi_x) - L_{13}(\Psi_y) + \gamma_{14}L_{14}(F) - \gamma_0\gamma_{14}\frac{\partial^2 F}{\partial x^2} - \gamma_{14}\beta^2\left(\lambda_x\frac{\partial^2 W}{\partial x^2} + \lambda_y\frac{\partial^2 W}{\partial y^2}\right)$$
$$= -\left(\ddot{W} + \hat{I}_7\frac{\partial^2 \ddot{W}}{\partial x^2} + \hat{I}_7'\beta^2\frac{\partial^2 \ddot{W}}{\partial y^2}\right) - \left(\hat{I}_5\frac{\partial \ddot{\Psi}_x}{\partial x} + \hat{I}_5'\beta\frac{\partial \ddot{\Psi}_y}{\partial y}\right), \tag{25}$$

$$L_{21}(F) + \gamma_{24}L_{22}(\Psi_x) + \gamma_{24}L_{23}(\Psi_y) - \gamma_{24}L_{24}(W) + \gamma_0\gamma_{24}\frac{\partial^2 W}{\partial x^2} = 0, \tag{26}$$

$$L_{31}(W) + L_{32}(\Psi_x) - L_{33}(\Psi_y) + \gamma_{14}L_{34}(F) = -\hat{I}_3\ddot{\Psi}_x + \hat{I}_5\frac{\partial \ddot{W}}{\partial x}, \tag{27}$$

$$L_{41}(W) - L_{42}(\Psi_x) + L_{43}(\Psi_y) + \gamma_{14}L_{44}(F) = -\hat{I}_3'\ddot{\Psi}_y + \hat{I}_5'\beta\frac{\partial \ddot{W}}{\partial y}. \tag{28}$$

In Eqs. (25)–(28) all the dimensionless operators can be found in Ref. [10].

The out-of-plane boundary conditions (15) and (16) become

$x = 0, 1$:

Simply supported (S):

$$W = 0,\ \ \delta_y = 0,\ \ \Psi_y = 0,\ \ M_x = 0,\ \ P_x = 0. \tag{29a}$$

Clamped (C):

$$W = 0,\ \ \delta_y = 0,\ \ \Psi_x = 0,\ \ \Psi_y = 0,\ \ \frac{\partial W}{\partial x} = 0. \tag{29b}$$

Free (F):

$$M_x = 0,\ \ P_x = 0,\ \ \delta_y = 0,$$
$$M_{xy}^* = M_{xy} - c_1 P_{xy} = 0,\ \ Q_x^* = Q_x - 3c_1 R_x - c_1\left(\frac{\partial P_x}{\partial x} + 2\beta\frac{\partial P_{xy}}{\partial y}\right) = 0. \tag{29c}$$

$y = 0, 1$:

Simply supported (S):

$$W = 0,\ \ \Psi_x = 0,\ \ M_y = 0,\ \ P_y = 0,\ \ \frac{\partial^2 F}{\partial x \partial y} = 0. \tag{30a}$$

Clamped (C):

$$W = 0,\ \ \Psi_x = 0,\ \ \Psi_y = 0,\ \ \frac{\partial W}{\partial y} = 0,\ \ \frac{\partial^2 F}{\partial x \partial y} = 0, \tag{30b}$$

and the dimensionless forms of the in-plane boundary conditions (17) are

$$x = 0, 1: \quad \int_0^1 \frac{\partial^2 F}{\partial y^2}\,\mathrm{d}y + \lambda_x = 0 \ \text{(movable)} \quad \text{or} \quad \delta_x = 0 \ \text{(immovable)}. \tag{31a}$$

$$y = 0, 1: \quad \int_0^1 \frac{\partial^2 F}{\partial x^2}\,\mathrm{d}x + \lambda_y = 0 \ \text{(movable)} \quad \text{or} \quad \delta_y = 0 \ \text{(immovable)}. \tag{31b}$$

The dimensionless end-shortening relationships can be rearranged as the sum of shortening deformations (δ_{xL}, δ_{yL}) due to mechanical load and those (δ_{xT}, δ_{yT}) due to thermal load

$$\delta_x = (\delta_{xL} - \delta_{xT}\lambda_T)/\gamma_{24}\beta^2, \quad \delta_y = (\delta_{yL} - \delta_{yT}\lambda_T)/\gamma_{24}\beta^2, \tag{32}$$

where

$$\delta_{xL} = -\int_0^1\int_0^1 \left[\gamma_{24}^2\beta^2\frac{\partial^2 F}{\partial y^2} - \gamma_5\frac{\partial^2 F}{\partial x^2} + \gamma_{24}\left(\gamma_{511}\frac{\partial \Psi_x}{\partial x} + \gamma_{233}\beta\frac{\partial \Psi_y}{\partial y}\right) - \gamma_{24}\left(\gamma_{p18}\frac{\partial^2 W}{\partial x^2} + \gamma_{p28}\beta^2\frac{\partial^2 W}{\partial y^2}\right)\right]\mathrm{d}x\,\mathrm{d}y,$$

$$\delta_{yL} = -\int_0^1\int_0^1 \left[\frac{\partial^2 F}{\partial x^2} - \gamma_5\beta^2\frac{\partial^2 F}{\partial y^2} + \gamma_{24}\left(\gamma_{512}\frac{\partial \Psi_x}{\partial x} + \gamma_{518}\beta\frac{\partial \Psi_y}{\partial y}\right) + \gamma_0\gamma_{24}W - \gamma_{24}\left(\gamma_{p16}\frac{\partial^2 W}{\partial x^2} + \gamma_{p26}\beta^2\frac{\partial^2 W}{\partial y^2}\right)\right]\mathrm{d}y\,\mathrm{d}x,$$

$$\delta_{xT} = -\frac{1}{\gamma_{24}\beta^2}\int_0^1\int_0^1 (\gamma_{24}^2\gamma_{T1} - \gamma_5\gamma_{T2})\,\mathrm{d}x\,\mathrm{d}y,$$

$$\delta_{yT} = -\frac{1}{\gamma_{24}\beta^2}\int_0^1\int_0^1 (\gamma_{T2} - \gamma_5\gamma_{T1})\,\mathrm{d}y\,\mathrm{d}x. \tag{33}$$

In the above equations dimensionless quantities γ_{ijk} are defined as in Appendix A.

3. Solution procedure

3.1. Semi-analytical DQ approximation

Similarly as in our previous work [13–15], a semi-analytical approach is used in the present analysis. According to the differential quadrature rule, solutions of W, F, Ψ_x and Ψ_y can be approximated along x-axis in terms of their function values at a number of pre-selected sampling points by

$$\{W, F, \Psi_x, \Psi_y\} = \sum_{j=1}^{N} l_j(x)\{W_j, F_j, \Psi_{xj}, \Psi_{yj}\}, \tag{34}$$

and their kth partial derivatives with respect to x at a sampling point x_i ($i = 1, \ldots, N$) can also be expressed as

$$\frac{\partial^k}{\partial x^k}\{W, F, \Psi_x, \Psi_y\}|_{x=x_i} = \sum_{j=1}^{N} C_{ij}^{(k)}\{W_j, F_j, \Psi_{xj}, \Psi_{yj}\}, \tag{35}$$

where

$$W_j = W(x_j, y, t), \quad F_j = F(x_j, y, t),$$
$$\Psi_{xj} = \Psi_x(x_j, y, t), \quad \Psi_{yj} = \Psi_y(x_j, y, t). \tag{36}$$

Recursive formula for weighting coefficient $C_{ij}^{(k)}$ and the Lagrange interpolation polynomial $l_j(x)$ can be found in Ref. [16]. The sampling point system in the present analysis is chosen to be the Chebyshev–Gauss–Lobatto spacing grid as

$$x_1 = 0.0, \quad x_2 = 0.0001, \quad x_j = \frac{1}{2}\left[1 - \cos\frac{\pi(j-2)}{N-3}\right],$$
$$x_{N-1} = 0.9999, \quad x_N = 1.0. \tag{37}$$

Applying Eqs. (34)–(37) to the governing equations (25)–(28) yields $4N$ sets of equations in terms of W_j, F_j, Ψ_{xj} and Ψ_{yj}, which are to be expanded in series forms as following:

$$W_j = \sum_{m=1}^{M} a_{jm}(t) W_{jm}(y), \tag{38a}$$

$$F_j = -\left(\frac{y^2}{2}\lambda_x + \frac{x^2}{2}\lambda_y\right) + \sum_{m=1}^{M} b_{jm}(t) F_{jm}(y), \tag{38b}$$

$$\Psi_{xj} = \sum_{m=1}^{M} c_{jm}(t) \Psi_{xjm}(y), \tag{38c}$$

$$\Psi_{yj} = \sum_{m=1}^{M} d_{jm}(t) \Psi_{yjm}(y), \tag{38d}$$

in which M denotes total number of truncated series, $a_{jm}(t)$, $b_{jm}(t)$, $c_{jm}(t)$ and $d_{jm}(t)$ stand for the generalized co-ordinates. W_{jm}, F_{jm}, Ψ_{xjm} and Ψ_{yjm} are to be modelled according to the associated boundary constraints at $y = 0, 1$, they are

Simply supported:

$$W_{jm} = \sin(m\pi y), \tag{39a}$$

$$F_{jm} = \sin\alpha_m y - \sinh\alpha_m y - \xi_m(\cos\alpha_m y - \cosh\alpha_m y), \tag{39b}$$

$$\Psi_{xjm} = \sin(m\pi y), \quad \Psi_{yjm} = \cos(m\pi y), \tag{39c}$$

Clamped:

$$W_{jm} = \sin\alpha_m y - \sinh\alpha_m y - \xi_m(\cos\alpha_m y - \cosh\alpha_m y), \tag{40a}$$

$$F_{jm} = \sin \alpha_m y - \sinh \alpha_m y - \xi_m(\cos \alpha_m y - \cosh \alpha_m y), \tag{40b}$$

$$\Psi_{xjm} = \sin(m\pi y), \quad \Psi_{yjm} = \sin(m\pi y), \tag{40c}$$

where $\xi_m = (\sin \alpha_m - \sinh \alpha_m)/(\cos \alpha_m - \cosh \alpha_m)$, $\alpha_m = (2m+1)\pi/2$.

Applying the Galerkin procedure after substituting Eq. (39) or (40) into the resulted $4N$ sets of equations leads to a linear algebraic system in matrix form as

$$\mathbf{M}\ddot{\boldsymbol{\eta}} + (\mathbf{K}_0 + \mathbf{K}_s + \mathbf{K}_d \cos \theta t)\boldsymbol{\eta} = \mathbf{0}, \tag{41}$$

where $\mathbf{M}$ is 'the mass matrix', $\mathbf{K}_0$ is 'the elastic stiffness matrix', $\mathbf{K}_s$ and $\mathbf{K}_d$ are 'the geometric stiffness matrices' associated with the static component λ_s and the oscillating component λ_d, respectively, $\boldsymbol{\eta}$ is composed of $a_{jm}(t)$, $b_{jm}(t)$, $c_{jm}(t)$ and $d_{jm}(t)$ at each nodal line.

3.2. Free vibration

Note that in the absence of λ_d, Eq. (41) reduces to an eigenvalue system for FGM cylindrical panels initially stressed by λ_s. Several methods can be used to obtain natural frequencies and corresponding modes [17]. To this end, it is assumed that

$$\boldsymbol{\eta}(t) = \bar{\boldsymbol{\eta}} e^{i\omega t}. \tag{42}$$

Substituting Eq. (42) into Eq. (41), we have

$$\{(\mathbf{K}_0 + \mathbf{K}_s) - \omega^2 \mathbf{M}\}\bar{\boldsymbol{\eta}} = \mathbf{0}, \tag{43}$$

where $\bar{\boldsymbol{\eta}}$ implies the corresponding mode shapes.

3.3. Parametric resonance

Eq. (41) is in the form of a second order differential equation with periodic coefficient of the Mathieu–Hill type, representing the dynamic stability problem of FGM panels under a periodic in-plane force. Several methods can be used to obtain points on the boundaries of the instability regions, such as Bolotin's method [18–28] and multiple scale method [29–31]. Here, Bolotin's method is used. The solutions can be sought in the following trigonometric series expansions:

$$\boldsymbol{\eta} = \sum_{k=1,3,\ldots}^{\infty} \left(\mathbf{a}_k \sin \frac{k\theta t}{2} + \mathbf{b}_k \cos \frac{k\theta t}{2} \right), \tag{44}$$

with period $2T_\theta$, where $T_\theta = 2\pi/\theta$, or

$$\boldsymbol{\eta} = \frac{1}{2}\mathbf{b}_0 + \sum_{k=2,4,\ldots}^{\infty} \left(\mathbf{a}_k \sin \frac{k\theta t}{2} + \mathbf{b}_k \cos \frac{k\theta t}{2} \right), \tag{45}$$

with period T_θ, $\mathbf{a}_k$ and $\mathbf{b}_k$ are arbitrary time-independent vectors. Our attention will be focused on the solutions with period $2T_\theta$ since the widths of these unstable regions are usually larger than those associated with the solutions with period T_θ and therefore are of greater practical importance. Substitution of series expansion (44) into Eq. (41) and a term-wise comparison of sine- and cosine-coefficients yields the following infinite systems of linear homogeneous algebraic

equations in terms of $\mathbf{a}_k$:

$$\left(\mathbf{K}_0 + \mathbf{K}_s - \frac{1}{2}\mathbf{K}_d - \frac{\theta^2}{4}\mathbf{M}\right)\mathbf{a}_1 + \frac{1}{2}\mathbf{K}_d\mathbf{a}_3 = \mathbf{0}, \tag{46a}$$

$$\left(\mathbf{K}_0 + \mathbf{K}_s - \frac{k^2\theta^2}{4}\mathbf{M}\right)\mathbf{a}_k + \frac{1}{2}\mathbf{K}_d(\mathbf{a}_{k-2} + \mathbf{a}_{k+2}) = \mathbf{0}, \quad k \geqslant 3 \tag{46b}$$

and in terms of $\mathbf{b}_k$:

$$\left(\mathbf{K}_0 + \mathbf{K}_s + \frac{1}{2}\mathbf{K}_d - \frac{\theta^2}{4}\mathbf{M}\right)\mathbf{b}_1 + \frac{1}{2}\mathbf{K}_d\mathbf{b}_3 = 0, \tag{47a}$$

$$\left(\mathbf{K}_0 + \mathbf{K}_s - \frac{k^2\theta^2}{4}\mathbf{M}\right)\mathbf{b}_k + \frac{1}{2}\mathbf{K}_d(\mathbf{b}_{k-2} + \mathbf{b}_{k+2}) = 0, \quad k \geqslant 3. \tag{47b}$$

For non-trivial solutions, the infinite determinants of these matrix equations should be equal to zero. Approximate solutions can be obtained by truncating the determinants, among which the so-called 'first approximation' with $k = 1$ is capable of getting solutions with sufficient accuracy. Therefore, the first approximation is used to determine the critical pulsating frequency θ through the following eigenvalue problems:

$$\left|\mathbf{K}_0 + \mathbf{K}_s - \frac{1}{2}\mathbf{K}_d - \frac{\theta^2}{4}\mathbf{M}\right| = \mathbf{0}, \tag{48a}$$

$$\left|\mathbf{K}_0 + \mathbf{K}_s + \frac{1}{2}\mathbf{K}_d - \frac{\theta^2}{4}\mathbf{M}\right| = \mathbf{0}, \tag{48b}$$

here each matrix comprises $4NM \times 4NM$ elements.

For a given axial load level, Eq. (48) delivers two critical excitation frequencies, thus determining the unstable region bounded by two curves with a common point when $\lambda_s = 0$.

Table 1
Dimensionless fundamental frequency of simply supported isotropic cylindrical panels

b/a	Present				Chern and Chao [33]	Kabayashi and Leissa [32]
	$N \times M =$ 9×5	$N \times M =$ 11×5	$N \times M =$ 13×5	$N \times M =$ 15×6		
0.5	1.31598	1.31597	1.31597	1.31597	1.31742	1.3360
1.0	0.55136	0.55136	0.55136	0.55136	0.55049	0.5563
1.5	0.40265	0.40266	0.40266	0.40266	0.39987	0.4044
2.0	0.35017	0.35019	0.35020	0.35019	0.34612	0.3505

4. Numerical results and discussions

4.1. Comparison studies

For the problem under consideration, there are no suitable comparison results of FGM panels in the literature. To ensure the efficiency and accuracy of the present methodology, three illustrative examples were solved for free vibration analysis and dynamic instability of homogeneous isotropic cylindrical panels.

Example 1. We first calculate the dimensionless fundamental frequencies $\omega^* = \Omega a\sqrt{\rho(1-\nu^2)/E}$ for simply supported isotropic cylindrical panels ($a/R = 0.1$, $a/h = 10$, $\nu = 0.3$) with varying aspect ratios ($b/a = 0.5, 1.0, 1.5, 2.0$). The results are listed in Table 1. The first order shear deformation shell theory solutions by Kobayashi and Leissa [32] and three-dimensional elasticity solutions by Chern and Chao [33] are also provided for direct comparisons. Excellent agreement is observed between the three.

Example 2. In Table 2, first seven natural frequencies of clamped isotropic aluminum cylindrical panels are presented, together with the experimental and finite element results obtained by Olson and Lindberg [34], the spline finite strip solutions by Cheung et al. [35] and three-dimensional elasticity solutions by Liew et al. [36] for comparison. The computation data are: $a = 4.0$ in, $b_0 = 3.0$ in, $R = 30.0$ in, $h = 0.013$ in, $E = 10^7$ psi, $\rho = 0.096$ lbf/in^3, $\nu = 0.3$, where b_0 is the chord length. Our results are in close agreement with the existing ones.

Example 3. We now turn our attention to the parametric resonance of simply supported, shear deformable isotropic cylindrical panel ($b_0/R = 0.5$, $a/R = 2$, $\nu = 0.3$) under combined static and periodic axial excitation. Results showed that, in this example, the two boundaries of each unstable region are basically straight lines that form a downward triangle. This makes it appropriate to define the unstable region by means of the point of origin and the subtending angle Θ. Tables 3 and 4 give, respectively, the first four unstable regions for panels ($h/R = 0.03$, 0.04, 0.05) under axial tensile load $\lambda_s = -0.5\lambda_{cr}$ and compressive load $\lambda_s = 0.5\lambda_{cr}$, where λ_{cr} is the critical buckling load of the panels. Comparisons have been made between the classical shell

Table 2
Natural frequencies of clamped isotropic cylindrical panels (in Hz)

Mode sequence	Exp. [34]	FEM [34]	FSM [35]	3-D [36]	Present ($N \times M$)			
					11×5	13×5	15×6	17×7
1	814	870	874	872.4	826.5	871.6	871.6	871.6
2	940	958	963	960.3	940.1	961.1	961.2	961.1
3	1260	1228	1298	1292.5	1196.6	1270.9	1280.5	1279.6
4	1306	1363	1369	1364.8	1295.8	1384.7	1370.4	1367.2
5	1452	1440	—	1443.0	1368.0	1463.4	1445.9	1446.3
6	1770	1756	—	1761.1	1708.2	1717.3	1761.1	1763.2
7	1802	1780	—	1786.8	1769.2	1812.0	1788.0	1782.4

Table 3
First four unstable regions of a simply supported isotropic cylindrical panel under axial tensile loading $\lambda_s = -0.5\lambda_{cr}$

Unstable regions	Point of origin θ^*				Angle subtended Θ			
	CST [37]	FSDT [37]	HSDT (Present)	Diff %	CST [37]	FSDT [37]	HSDT (Present)	Diff %
$h/R = 0.03$								
First	0.7650871	0.7605915	0.7545067	0.80	0.0256951	0.0258446	0.0260106	0.64
Second	1.0722443	1.0664572	1.0589919	0.70	0.0726175	0.0729988	0.0733171	0.44
Third	1.5076184	1.4988417	1.4883498	0.71	0.1162854	0.1169408	0.1176410	0.60
Fouth	1.9975838	1.9832372	1.9634048	1.00	0.1567566	0.1578453	0.1592543	0.89
$h/R = 0.04$								
First	0.9976844	0.9870142	0.9810921	0.60	0.0263148	0.0265958	0.0267864	0.71
Second	1.3274792	1.3235779	1.3116656	0.90	0.0777726	0.0785666	0.0792208	0.87
Third	1.8313471	1.8102993	1.7921963	1.00	0.1277765	0.1292115	0.1306461	1.11
Fourth	2.4111464	2.3769167	2.3521475	1.48	0.1732664	0.1756690	0.1785070	1.61
$h/R = 0.05$								
First	1.2308019	1.2100794	1.1958189	1.18	0.0266880	0.0271407	0.0274425	1.10
Second	1.6062721	1.5790699	1.5548582	1.53	0.0810604	0.0824241	0.0835097	1.32
Third	2.1621062	2.1209467	2.0876162	1.58	0.1354157	0.1379647	0.1398180	1.43
Fourth	2.8345409	2.7679303	2.7028754	2.35	0.1843507	0.1886388	0.1929011	2.26

Table 4
First four unstable regions for a simply supported isotropic cylindrical panel under axial compressive loading $\lambda_s = 0.5\lambda_{cr}$

Unstable regions	Point of origin θ^*				Angle subtended Θ			
	CST [37]	FSDT [37]	HSDT (Present)	Diff %	CST [37]	FSDT [37]	HSDT (Present)	Diff %
$h/R = 0.03$								
First	0.6532618	0.6483488	0.6415411	1.05	0.0300034	0.0302256	0.0304976	0.90
Second	0.7182320	0.7110948	0.7014239	1.36	0.1062933	0.1072842	0.1083463	0.99
Third	0.9171988	0.9060940	0.8914153	1.62	0.1852367	0.1872843	0.1898126	1.35
Fourth	1.1957598	1.1776127	1.1562979	1.81	0.2528890	0.2563688	0.2602399	1.51
$h/R = 0.04$								
First	0.8854011	0.8739775	0.8627906	1.28	0.0296026	0.0299832	0.0303579	1.25
Second	0.9715799	0.9549933	0.9412414	1.44	0.1057441	0.1074819	0.1089544	1.37
Third	1.2023632	1.1760791	1.1529103	1.97	0.1903083	0.1942196	0.1979098	1.90
Fourth	1.5495172	1.5063851	1.4718888	2.29	0.2626528	0.2694866	0.2752536	2.14
$h/R = 0.05$								
First	1.1183180	1.0964077	1.0760145	1.86	0.0293425	0.0299214	0.0304390	1.73
Second	1.2346733	1.2030459	1.1769398	2.17	0.1045971	0.1072303	0.1093749	2.00
Third	1.5135089	1.4632239	1.4238632	2.69	0.1904003	0.1965104	0.2013249	2.45
Fourth	1.9419439	1.8595201	1.8046643	2.95	0.2639889	0.2747844	0.2822311	2.71

solutions (CST), the first shear deformation shell theory solutions (FSDT) by Ng et al. [37] and the present ones (HSDT). Again, excellent correlation is achieved.

In Tables 3 and 4, the percentage differences (diff. %) between the FSDT results and HSDT results are also displayed. As expected, compared with CST and FSDT results, the present HSDT formulation produces more conservative points of origin and wider unstable regions as the panel becomes thicker. The differences increase as h/R is increased. This is due to the fact that the transverse shear and rotary inertia will have more effect on a thicker panel. It is also worthwhile to note that, in the present analysis, only two $4NM$-order eigenvalue systems in Eq. (48) are to be solved to define the unstable regions.

Convergence studies are also undertaken in both Tables 1 and 2 by increasing N and M. Results show that the present method is well converged to produce results with sufficient accuracy when $N \geqslant 15$ and $M \geqslant 6$. Thus, $N \times M = 15 \times 6$ has been used in all the following computations.

4.2. Free vibration results

In what follows, parametric studies are carried out to supply information on both free vibration and parametric resonance of shear deformable FGM cylindrical panels subjected to combined thermal and mechanical loading. To this end, silicon nitride and stainless steel are chosen to be the constituent materials of the FGM panel, referred to as Si_3N_4/SUS304. Their material properties P, such as Young's modulus E, the Poisson ratio v, coefficient of thermal expansion α, are temperature dependent and can be expressed as [38]

$$P = P_0(P_{-1}T^{-1} + 1 + P_1T + P_2T^2 + P_3T^3), \tag{49}$$

in which $T = T_0 + \Delta T$, P_0, P_{-1}, P_1, P_2 and P_3 are the coefficients of temperature T (K) and are unique to each constituent. Typical values for silicon nitride and stainless steel are listed in Table 5.

For the sake of brevity, a clockwise notation starting from $y = 0$ is employed. Symbol 'CSCF', for example, identifies a panel clamped at $y = 0, 1$, simply supported at $x = 0$, and free at $x = 1$. In Tables 6 and 7 and Fig. 2, $\omega^* = \Omega a^2\sqrt{\rho_0 h/D_0}$ refers to the dimensionless natural frequencies of

Table 5
Temperature-dependent coefficients of elastic modulus E (GPa), the Poisson ratio v, mass density ρ (kg/m^3) and linear thermal expansion α (1/K) for ceramic and metal

	Material	P_{-1}	P_0	P_1	P_2	P_3	P (at $T = 300$ K)
E	SUS304	0	201.04e9	3.079e–4	−6.534e–7	0	207.7877e9
	Si_3N_4	0	348.43e9	−3.070e–4	2.160e–7	−8.946e–11	322.2715e9
v	SUS304	0	0.3262	−2.002e–4	3.797e–7	0	0.31776
	Si_3N_4	0	0.2400	0	0	0	0.24000
α	SUS304	0	12.330e–6	8.086e–4	0	0	15.3210e–6
	Si_3N_4	0	5.8723e–6	9.095e–4	0	0	7.4745e–6
ρ	SUS304	0	8166	0	0	0	8166
	Si_3N_4	0	2370	0	0	0	2370

Table 6
Dimensionless frequency parameters ω^* for clamped, thermo-mechanically pre-stressed FGM cylindrical panels movable at $x = 0, 1$

Material composition	$\Delta T = 0$				$\Delta T = 300\,\mathrm{K}$			
	1	2	3	4	1	2	3	4
Without axial load								
Si_3N_4	74.518	144.663	145.740	206.992	72.446	140.642	141.687	201.238
$n = 0.2$	57.479	111.717	112.531	159.855	55.739	108.338	109.126	155.010
$n = 2.0$	40.750	78.817	79.407	112.457	39.369	76.106	76.675	108.541
$n = 10.0$	35.852	69.075	69.609	98.386	34.571	66.539	67.055	94.709
SUS304	32.761	63.314	63.806	90.370	31.511	60.846	61.321	86.805
Under axial tension $\lambda_x = -5\pi^2$								
Si_3N_4	95.203	163.281	179.996	236.973	92.556	158.741	174.993	230.386
$n = 0.2$	73.571	126.379	138.967	183.126	71.374	122.620	134.782	177.625
$n = 2.0$	52.572	90.067	98.600	129.770	50.875	87.153	95.292	125.419
$n = 10.0$	46.472	79.421	86.760	114.067	44.924	76.747	83.699	110.035
SUS304	42.463	72.828	79.342	104.614	40.950	70.229	76.355	100.697
Under axial compression $\lambda_x = 5\pi^2$								
Si_3N_4	42.592	95.435	125.338	171.210	41.405	92.782	121.851	166.450
$n = 0.2$	32.558	73.784	96.379	132.061	31.502	71.517	93.377	127.989
$n = 2.0$	22.030	50.936	66.809	91.562	21.066	49.015	64.257	88.133
$n = 10.0$	18.783	43.925	57.918	79.330	17.811	42.054	55.457	76.028
SUS304	17.212	40.645	53.058	73.106	16.268	38.847	50.659	69.917

the FGM cylindrical panels. ρ_0 and D_0, selected to be ρ of stainless steel and the D_{11}^* of pure stainless-steel panel ($a/h = 10$) at $T_0 = 300\,\mathrm{K}$, serve as the reference values of mass density and D_{11}^*, respectively.

Table 6 gives the first four dimensionless natural frequencies of clamped FGM cylindrical panels ($a/R = 0.1$, $a/h = 10$, $a = b$) movable at $x = 0, 1$, with various material compositions and initially stressed by different thermo-mechanical loadings. The fully Si_3N_4 and SUS304 cases correspond to isotropic plates in nature, while the other three cases ($n = 0.2, 2.0, 10.0$) are for the graded panels with two constituent materials. It is obvious from Table 5 that the bending stiffness is the maximum for the ceramic panel, the minimum for the metallic panel, and degrades gradually as the volume fraction index n increases. Three sets of mechanical loads are considered, including $\lambda_x = 0$ for no in-plane loads, $\lambda_x = -5\pi^2$ for axial stretching and $\lambda_x = 5\pi^2$ for axial compression. The thermal loading is due to uniform temperature rise $\Delta T = 0$ and $300\,\mathrm{K}$. It is observed that, both initial axial compression and temperature rise will result in a decrease in the natural frequency ω^*. In contrast, an initial axial tension will help increase the natural frequency. Among the FGM panels, the fully silicon nitride one has the highest ω^* while its fully stainless-steel counterpart has the lowest ω^*. Moreover, ω^* decreases as the volume fraction index n increases.

Table 7 compares the first eight dimensionless frequencies of FGM cylindrical panels ($a/R = 0.1$, $a/h = 10$, $a/b = 1.0, 2.0$, $n = 0.2, 2.0$) with different boundary conditions (CCCC,

Table 7
Dimensionless frequency parameters ω^* of FGM cylindrical panels movable at $x = 0, 1$ and under uniform temperature change $\Delta T = 300\,\mathrm{K}$

Boundary conditions	a/b	n	Mode sequence							
			1	2	3	4	5	6	7	8
CCCC	1.0	0.2	55.739	108.338	109.126	155.010	172.031	183.588	213.659	224.500
		2.0	39.369	76.106	76.675	108.541	122.134	128.227	150.744	156.468
	2.0	0.2	136.982	173.924	236.411	312.216	318.897	343.103	394.384	414.717
		2.0	95.728	121.397	164.501	215.687	220.969	236.875	271.816	286.152
CSCC	1.0	0.2	49.748	95.994	106.266	146.968	167.888	170.421	208.271	212.645
		2.0	35.196	67.666	74.709	103.101	117.718	121.056	147.180	148.596
	2.0	0.2	134.689	166.712	225.027	305.234	311.332	339.991	388.655	401.580
		2.0	94.136	116.485	156.916	212.032	215.096	234.814	268.078	277.582
CSCS	1.0	0.2	45.426	84.741	104.006	139.840	152.513	168.917	201.219	203.424
		2.0	32.168	59.909	73.149	98.244	107.342	120.062	140.967	143.953
	2.0	0.2	132.934	160.431	214.131	291.749	310.548	337.165	383.200	387.586
		2.0	92.914	112.174	149.608	203.174	214.569	232.933	264.505	268.511
CFCF	1.0	0.2	35.182	41.517	66.856	92.537	101.326	120.071	129.228	157.980
		2.0	24.881	29.139	47.162	65.017	70.885	84.830	90.520	112.299
	2.0	0.2	125.100	130.575	150.472	191.820	256.154	300.656	307.389	330.212
		2.0	87.362	90.986	105.009	134.112	179.325	207.612	212.087	228.056
CSCF	1.0	0.2	36.996	55.284	95.012	101.745	115.432	158.729	160.566	174.568
		2.0	26.111	39.018	66.694	71.872	80.970	111.316	114.046	122.955
	2.0	0.2	126.662	140.698	175.318	234.905	302.686	316.688	319.094	352.586
		2.0	88.412	98.222	122.539	164.222	208.980	220.382	220.841	243.545

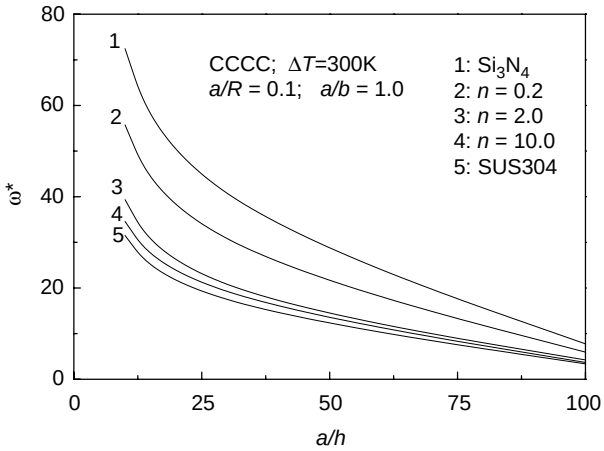

Fig. 2. Relationships of fundamental frequency with side-to-thickness ratio for Si_3N_4/SUS304 cylindrical panels under uniform temperature rise.

CSCC, CSCS, CFCF, CSCF), movable at $x = 0$, 1, free from in-plane load and under uniform temperature rise $\Delta T = 300$ K. Results show that the fully clamped cylindrical panel has the highest, whereas the CFCF one has the lowest natural frequency values, implying that an FGM panel with greater supporting rigidity will have higher vibrating frequencies. Meanwhile, a dramatic increase in ω^* takes place as β increases from 1.0 to 2.0.

Fig. 2 depicts variation of fundamental frequency of completely immovable, clamped FGM cylindrical panels ($a/R = 0.1, a/b = 1.0$) with varying side-to-thickness ratio a/h and under uniform temperature rise $\Delta T = 300 : \mathrm{K}$. As can be seen, the frequency is greatly influenced in that ω^* decreases steadily as a/h becomes larger, indicating that a thicker panel possesses higher vibrating frequencies.

4.3. Parametric resonance results

In the following numerical illustrations, parametric resonance of Si_3N_4/SUS304 cylindrical panels ($a/R = 0.2$) under combined static and periodic axial load and in thermal environments is investigated. Typical results are plotted in Figs. 3–8. It is preferred that $\alpha_d = \lambda_d/\lambda_s$ and $\theta^* = \theta a^2\sqrt{\rho_0 h/D_0}$ are used as dynamic load level and the dimensionless excitation frequency.

In Figs. 4–8, the volume fraction index $n = 0.2$, 2.0; in Figs. 3 and 5–8, the panel is clamped; in Figs. 3, 4 and 6–8, the panel is undergoing a uniform temperature rise $\Delta T = 300$ K; in Figs. 3–5, 7 and 8, $a/h = 10$; in Figs. 3–6 and 8, $a/b = 1.0$. In all examples, the panel is initially loaded by an axial compression $\lambda_s = 2\pi^2$. Except in Fig. 8, the panel is movable at $x = 0, 1$ and immovable at the other two sides.

Fig. 3 gives the unstable regions of thermo-mechanically stressed clamped FGM cylindrical panels with various volume fraction index n. The point of origin tends to be lower and the unstable region becomes narrower as n increases. This is due to the fact that the bending stiffness is the maximum for the ceramic panel, the minimum for the metallic panel, and degrades gradually as n increases.

To investigate the effect of out-of-plane boundary condition on the dynamic instability of thermo-mechanically stressed FGM cylindrical panels, unstable regions are plotted and compared

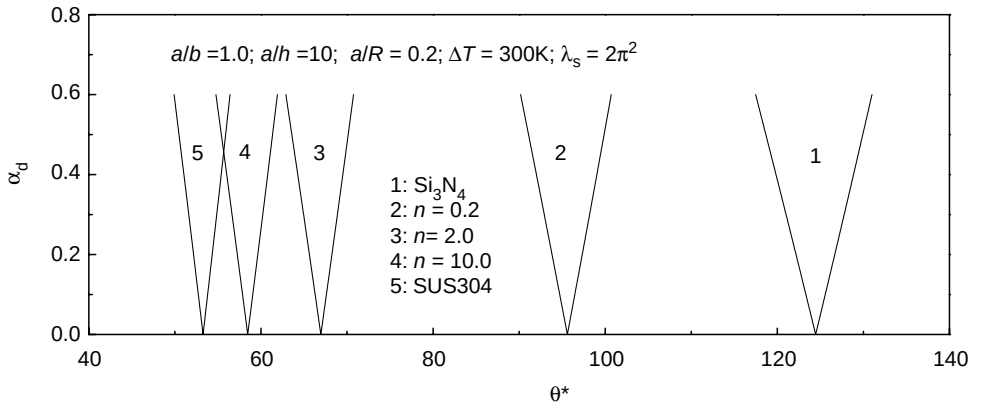

Fig. 3. Principal unstable regions of clamped Si_3N_4/SUS304 cylindrical panels with different material compositions.

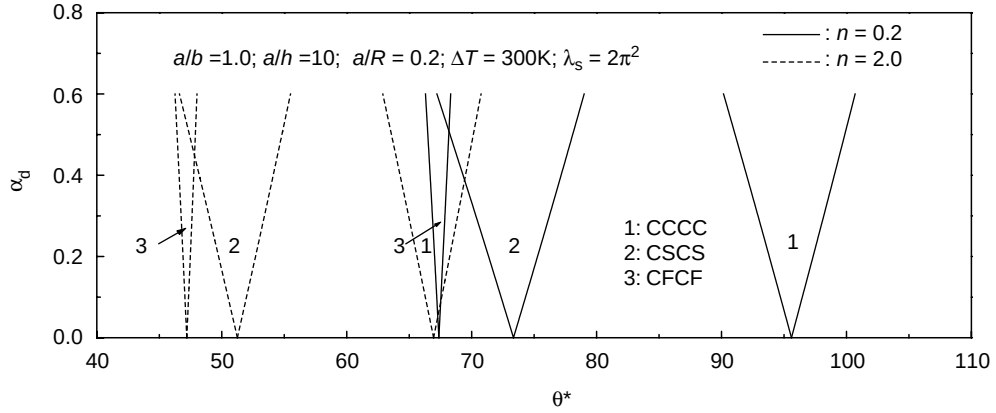

Fig. 4. Principal unstable regions of Si_3N_4/SUS304 cylindrical panels with different out-of-plane boundary conditions and under uniform temperature rise.

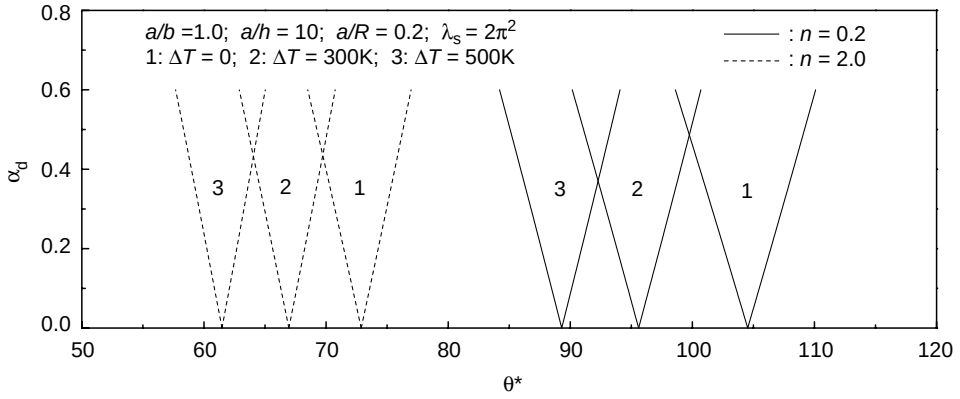

Fig. 5. Effect of temperature change on the principal unstable region of clamped Si_3N_4/SUS304 cylindrical panels.

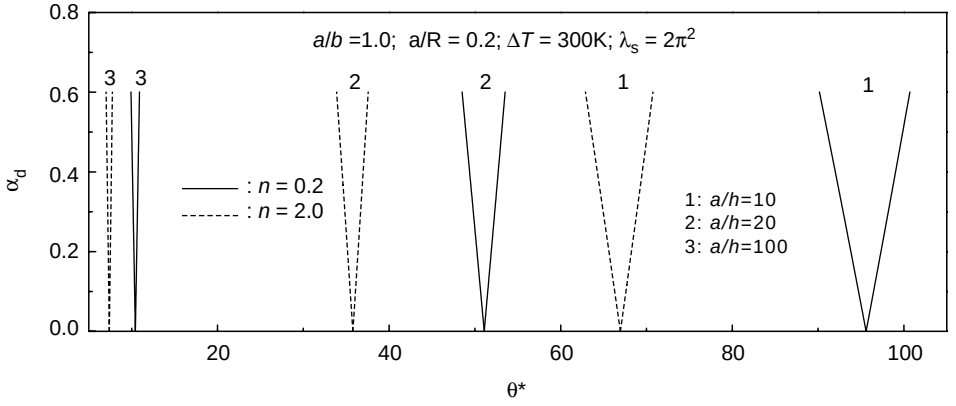

Fig. 6. Effect of side-to-thickness ratio on the principal unstable regions of clamped Si_3N_4/SUS304 cylindrical panels.

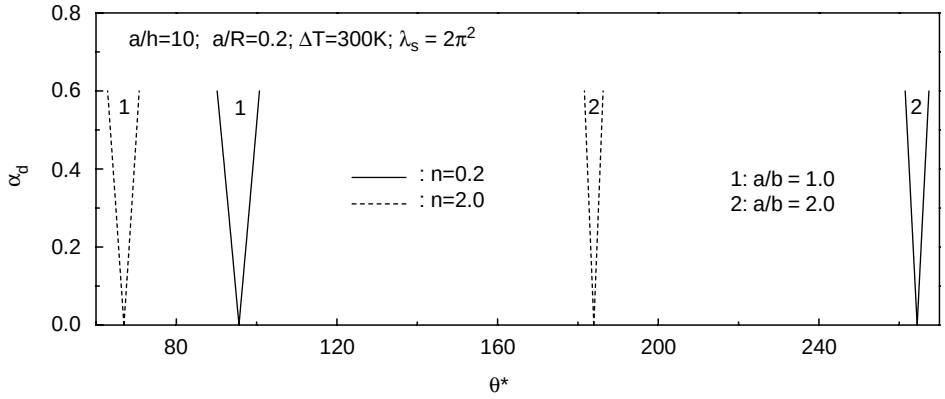

Fig. 7. Effect of aspect ratio on the principal unstable region of clamped Si_3N_4/SUS304 cylindrical panels.

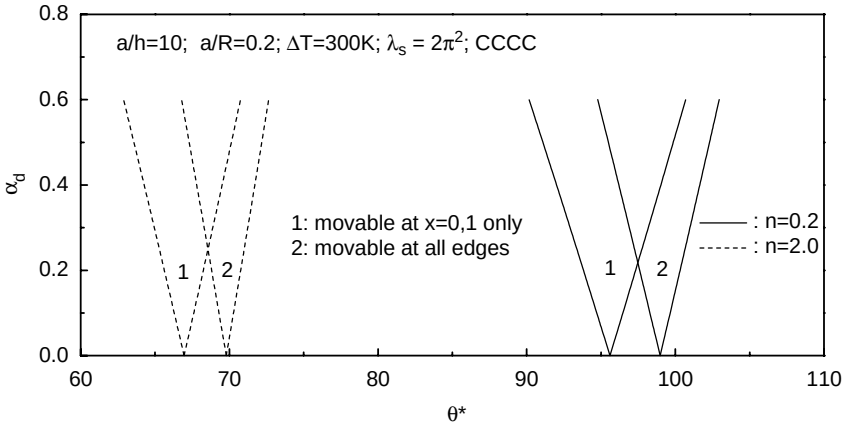

Fig. 8. Effect of in-plane boundary constraints on the principal unstable region of clamped Si_3N_4/SUS304 cylindrical panels.

in Fig. 4 for CCCC, CSCS, and CFCF panels. Results demonstrate that the panel with two opposite free edges, namely, CFCF panel, has the lowest point of origin and smallest unstable region, and a fully clamped has the highest point of origin and largest unstable region. Noteworthy is that the unstable regions are almost the same for CCCC and CSCS panels although the latter has much lower point of origin.

Fig. 5 shows the significant effect of temperature change on the dynamic instability of FGM cylindrical panels under initial thermo-mechanical loading. The temperature rise is chosen to be $\Delta T = 0$, 300 and 500 K. As expected, the unstable region moves to the left as temperature rises. This is due to more degradation in panel stiffness under higher environment temperature.

In Fig. 6, we examine the effect of side-to-thickness ratio on dynamic instability of FGM cylindrical panels. For this purpose, the side-to-thickness ratio is chosen as $a/h = 10$, 20 and 100. Results indicate that the points of origin decrease dramatically and the unstable regions are greatly narrowed as a/h changes from 10 to 100, i.e., as the panel becomes thinner.

Effect of panel aspect ratio β on parametric resonance of thermo-mechanically stressed FGM cylindrical panels is investigated in Fig. 7. It is found that the points of origin become much greater when $\beta = 2.0$. However, the corresponding unstable regions become a little smaller.

In Fig. 8, unstable regions of clamped FGM cylindrical panels with all edges movable and those movable at $x = 0, 1$ only are compared. It is observed that in-plane boundary conditions do have some influence, though not so significant, on parametric resonance of thermo-mechanically stressed FGM cylindrical panels.

5. Conclusions

Both free vibration and parametric resonance of FGM cylindrical panels subjected to thermo-mechanical loads have been investigated in this paper. Theoretical formulations are based on Reddy's higher order shear deformation shell theory to account for rotary inertias and parabolic distribution of the transverse shear strains through the panel thickness. Thermo-mechanical load consists of a steady temperature change, static and periodically pulsating forces in axial direction. Non-linear temperature dependency of material properties is also taken into account. A semi-analytical approach, which makes use of differential quadrature approximation and Galerkin technique, has been developed to obtain the natural frequency parameters of FGM panels. In the presence of dynamic axial loading, unstable regions are determined by using Bolotin's method. Numerical results for silicon nitride/stainless-steel cylindrical panels are presented in both tabular and graphical forms. A parametric study is also carried out, highlighting the effects of material composition, boundary conditions, initial thermal and/or mechanical axial loads as well as the panel geometry parameters on the dynamic characteristics. Results presented herein for FGM cylindrical panels are not available in the literature, and therefore, should be of interest to the engineering community.

Acknowledgements

This work is supported in part by the National Natural Science Foundation of China under Grant 59975058. The authors are grateful for this financial support.

Appendix A

$$(\gamma_{110}, \gamma_{112}, \gamma_{114}) = c_1[F_{11}^*, (F_{12}^* + F_{21}^* + 4F_{66}^*)/2, F_{22}^*]/D_{11}^*,$$

$$(\gamma_{120}, \gamma_{122}) = [(D_{11}^* - c_1F_{11}^*), (D_{12}^* - c_1F_{12}^* + 2D_{66}^* - 2c_1F_{66}^*)]/D_{11}^*,$$

$$(\gamma_{131}, \gamma_{133}) = [(D_{12}^* - c_1F_{21}^* + 2D_{66}^* - 2c_1F_{66}^*), (D_{22}^* - c_1F_{22}^*)]/D_{11}^*,$$

$$(\gamma_{140}, \gamma_{142}, \gamma_{144}) = c_1[B_{21}^*, (B_{11}^* + B_{22}^* - 2B_{66}^*), B_{12}^*]/(D_{11}^*D_{22}^*A_{11}^*A_{22}^*)^{1/4},$$

$$(\gamma_{212}, \gamma_{214}) = [(2A_{12}^* + A_{66}^*)/2, A_{11}^*]/A_{22}^*,$$

$$(\gamma_{220}, \gamma_{222}) = [(B^*_{21} - c_1 E^*_{21}), B^*_{11} - B^*_{66} - c_1(E^*_{11} - E^*_{66})]/(D^*_{11} D^*_{22} A^*_{11} A^*_{22})^{1/4},$$

$$(\gamma_{231}, \gamma_{233}) = [B^*_{22} - B^*_{66} - c_1(E^*_{22} - E^*_{66}), (B^*_{12} - c_1 E^*_{12})]/(D^*_{11} D^*_{22} A^*_{11} A^*_{22})^{1/4},$$

$$(\gamma_{240}, \gamma_{242}, \gamma_{244}) = c_1[E^*_{21}, (E^*_{11} + E^*_{22} - 2E^*_{66}), E^*_{12}]/(D^*_{11} D^*_{22} A^*_{11} A^*_{22})^{1/4}$$

$$(\gamma_{310}, \gamma_{312}) = c_1[(F^*_{11} - c_1 H^*_{11}), (F^*_{21} + 2F^*_{66} - c_1(H^*_{12} + 2H^*_{66}))]/(D^*_{11} D^*_{22} A^*_{11} A^*_{22})^{1/4},$$

$$(\gamma_{320}, \gamma_{322}, \gamma_{331}) = [(D^*_{11} - 2c_1 F^*_{11} + c_1^2 H^*_{11}), (D^*_{66} - 2c_1 F^*_{66} + c_1^2 H^*_{66}), D^*_{12} + D^*_{66} - c_1(F^*_{12} + F^*_{21} + 2F^*_{66}) + c_1^2(H^*_{12} + H^*_{66})]/D^*_{11},$$

$$(\gamma_{411}, \gamma_{413}) = c_1[F^*_{12} + 2F^*_{66} - c_1(H^*_{12} + 2H^*_{66}), F^*_{22} - c_1 H^*_{22}]/(D^*_{11} D^*_{22} A^*_{11} A^*_{22})^{1/4},$$

$$(\gamma_{430}, \gamma_{432}) = [(D^*_{66} - 2c_1 F^*_{66} + c_1^2 H^*_{66}), (D^*_{22} - 2c_1 F^*_{22} + c_1^2 H^*_{22})]/D^*_{11},$$

$$(\gamma_{31}, \gamma_{41}) = [(A^*_{55} - 6c_1 D^*_{55} + 9c_1^2 F^*_{55}), (A^*_{44} - 6c_1 D^*_{44} + 9c_1^2 F^*_{44})]/D^*_{11},$$

$$(\gamma_{511}, \gamma_{512}, \gamma_{517}, \gamma_{518}) = [B^*_{11} - c_1 E^*_{11}, B^*_{21} - c_1 E^*_{21}, B^*_{12} - c_1 E^*_{12}, B^*_{22} - c_1 E^*_{22}]/(D^*_{11} D^*_{22} A^*_{11} A^*_{22})^{1/4}$$

$$(\gamma_{p16}, \gamma_{p18}, \gamma_{p26}, \gamma_{p28}) = c_1(E^*_{21}, E^*_{11}, E^*_{22}, E^*_{12})/(D^*_{11} D^*_{22} A^*_{11} A^*_{22})^{1/4}, \tag{A.1}$$

where $\bar{S}^{\mathrm{T}} = \bar{M}^{\mathrm{T}} - c_1 \bar{P}^{\mathrm{T}}$.

References

[1] M. Yamanoushi, M. Koizumi, T. Hiraii, I. Shiota (Eds.), Proceedings of the First International Symposium on Functionally Gradient Materials, Sendai, Japan, 1990.

[2] M. Koizumi, The concept of FGM, Ceramic Transactions, Functionally Gradient Materials 34 (1993) 3–10.

[3] C.T. Loy, K.Y. Lam, J.N. Reddy, Vibration of functionally graded cylindrical shells, International Journal of Mechanical Sciences 41 (1999) 309–324.

[4] S.C. Pradhan, C.T. Loy, K.Y. Lam, J.N. Reddy, Vibration characteristics of functionally graded cylindrical shells under various boundary conditions, Applied Acoustics 61 (2000) 119–129.

[5] S.W. Gong, K.Y. Lam, J.N. Reddy, The elastic response of functionally graded cylindrical shells to low-velocity impact, International Journal of Impact Engineering 22 (1999) 397–417.

[6] X. Han, G.R. Liu, Z.C. Xi, K.Y. Lam, Transient waves in a functionally graded cylinder, International Journal of Solids and Structures 38 (2001) 3021–3037.

[7] T.Y. Ng, K.M. Lam, K.M. Liew, J.N. Reddy, Dynamic stability analysis of functionally graded cylindrical shells under periodic axial loading, International Journal of Solids and Structures 38 (2001) 1295–1309.

[8] J.N. Reddy, C.F. Liu, A higher-order shear deformation theory of laminated elastic shells, International Journal of Engineering Science 23 (1985) 319–330.

[9] A.K. Noor, W.S. Burton, Computational models for high-temperature multilayered composite plates and shells, Applied Mechanics Reviews 45 (1992) 419–445.

[10] H.S. Shen, Nonlinear bending response of functionally graded plates subjected to transverse loads and in thermal environments, International Journal of Mechanical Sciences 44 (2002) 561–584.

[11] H.S. Shen, Postbuckling of shear deformable cross-ply laminated cylindrical shells under combined external pressure and axial compression, International Journal of Mechanical Sciences 43 (2001) 2493–2523.

[12] H.S. Shen, Postbuckling of shear deformable laminated cylindrical shells, Journal of Engineering Mechanics American Society of Civil Engineers 128 (2002) 296–307.

[13] J. Yang, H.S. Shen, Dynamic response of initially stressed functionally graded rectangular plates resting on elastic foundations, Composite Structures 54 (2001) 497–508.
[14] J. Yang, H.S. Shen, Non-linear analysis of functionally graded plates under transverse and in-plane loads, International Journal of Non-Linear Mechanics 38 (2003) 467–482.
[15] J. Yang, H.S. Shen, Vibration characteristics and transient response of shear deformable functionally graded plates in thermal environment, Journal of Sound and Vibration 255 (2002) 579–602.
[16] C.W. Bert, D. Malik, Free vibration analysis of thin cylindrical shells by the differential quadrature method, Journal of Pressure Vessel Technology American Society of Mechanical Engineers 118 (1996) 1–12.
[17] Q.S. Li, Exact solutions for free vibration of shear type structures with arbitrary distribution of mass or stiffness, The Journal of The Acoustical Society of America 110 (2001) 1958–1966.
[18] V.V. Bolotin, The Dynamic Stability of Elastic System, Holden-Day, San Francisco, 1964.
[19] Y. Basar, C. Eller, W.B. Krätzig, Finite element procedures for parametric resonance phenomena of arbitrary elastic shell structures, Computational Mechanics 2 (1987) 89–98.
[20] J. Moorthy, J.N. Reddy, R.H. Plaut, Parametric instability of laminated composite plates with transverse shear deformation, International Journal of Solids and Structures 26 (1990) 801–811.
[21] G. Ganapathi, V. Balamurugan, Dynamic instability analysis of a laminated composite circular cylindrical shell, Computers and Structures 69 (1998) 181–189.
[22] G. Ganapathi, T.K. Varadnan, V. Balamurugan, Dynamic instability of laminated composite curved panels using finite element method, Computers and Structures 53 (1994) 335–342.
[23] T.Y. Ng, K.Y. Lam, J.N. Reddy, Dynamic stability of cross-ply laminated composite cylindrical shells, International Journal of Mechanical Sciences 20 (1998) 805–823.
[24] L. Librescu, S. Thangjitham, Parametric instability of laminated composite shear deformable flat panels subjected to in-plane edge loads, International Journal of Non-Linear Mechanics 25 (1990) 263–273.
[25] T.Y. Ng, K.Y. Lam, J.N. Reddy, Parametric resonance of a rotating cylindrical shell subjected to periodic loads, Journal of Sound and Vibration 214 (1998) 513–529.
[26] T.Y. Ng, K.Y. Lam, Effects of boundary conditions on the parametric resonance of cylindrical shells under axial loading, Shock and Vibration 5 (1998) 343–354.
[27] T.Y. Ng, H. Li, K.Y. Lam, C.T. Loy, Parametric instability of conical shells by the generalized differential quadrature method, International Journal for Numerical Methods in Engineering 44 (1999) 819–837.
[28] T.Y. Ng, K.Y. Lam, Parametric stability analysis of cross-ply laminated cylindrical shells using different thin shell theories, Acta Mechanica 134 (1999) 147–167.
[29] G. Cederbaum, Analysis of parametrically excited laminated shells, International Journal of Mechanical Sciences 34 (1992) 241–250.
[30] T.C.K. Molyneaux, L.Y. Li, Instability of cylindrical panels under combined static and dynamic loads, International Journal of Pressure Vessels and Piping 65 (1996) 163–169.
[31] A.A. Popov, J.M.T. Thompson, J.G.A. Croll, Bifurcation analyses in the parametrically excited vibrations of cylindrical panels, Nonlinear Dynamics 17 (1998) 205–225.
[32] Y. Kobayashi, A.W. Leissa, Large amplitude free vibration of thick shallow shells supported by shear diaphragms, International Journal of Non-Linear Mechanics 30 (1995) 57–66.
[33] Y.C. Chern, C.C. Chao, Comparison of natural frequencies of laminates by 3-D theory, Part II: curved panels, Journal of Sound and Vibration 230 (2000) 1009–1030.
[34] M.D. Olson, G.M. Lindberg, Dynamic analysis of shallow shell with a doubly-curved triangular finite element, Journal of Sound and Vibration 19 (1971) 299–318.
[35] Y.K. Cheung, W.Y. Li, L.G. Tham, Free vibration analysis of singly curved shell by the spline finite strip method, Journal of Sound and Vibration 128 (1989) 411–422.
[36] K.M. Liew, L.A. Bergman, T.Y. Ng, K.Y. Lam, Three-dimensional vibration of cylindrical shell panels-solution by continuum and discrete approaches, Computational Mechanics 26 (2000) 208–221.
[37] T.Y. Ng, K.Y. Lam, J.N. Reddy, Dynamic stability of cylindrical panels with transverse shear effects, International Journal of Solids and Structures 36 (1999) 3483–3496.
[38] Y.S. Touloukian, Thermophysical Properties of High Temperature Solid Materials, McMillan, New York, 1967.